

Article

A Novel Cogging Torque Simulation Method for Permanent-Magnet Synchronous Machines

Chun-Yu Hsiao *, Sheng-Nian Yeh and Jonq-Chin Hwang

Department of Electrical Engineering, National Taiwan University of Science and Technology, Taipei 10607, Taiwan; E-Mails: snyeh@mail.ntust.edu.tw (S.-N.Y.); jchwang@ee.ntust.edu.tw (J.-C.H.)

* Author to whom correspondence should be addressed; E-Mail: D9607101@mail.ntust.edu.tw; Tel.: +886-921135781; Fax: +886-2-27376699.

Received: 16 September 2011; in revised form: 22 November 2011 / Accepted: 30 November 2011 / Published: 6 December 2011

Abstract: Cogging torque exists between rotor mounted permanent magnets and stator teeth due to magnetic attraction and this is an undesired phenomenon which produces output ripple, vibration and noise in machines. The purpose of this paper is to study the existence and effects of cogging torque, and to present a novel, rapid, half magnet pole pair technique for forecasting and evaluating cogging torque. The technique uses the finite element method as well as Matlab research and development oriented software tools to reduce numerous computing jobs and simulation time. An example of a rotor-skewed structure used to reduce cogging torque of permanent magnet synchronous machines is evaluated and compared with a conventional analysis method for the same motor to verify the effectiveness of the proposed approach. The novel method is proved valuable and suitable for large-capacity machine design.

Keywords: cogging torque; permanent magnet; finite element method; half magnet pole pair

1. Introduction

Permanent magnet synchronous machines (PMSMs) are less noisy, highly efficient and have long life spans. Differences in permeability between the permanent magnet and the rotor magnetic core structure form an apparent protruding magnetic field distribution, which in turn produces the reluctance torque during synchronous operation. It has been used in a wide variety of industrial

application systems, such as aviation, electrical vehicles, home appliances, and high precision control instruments [1–4]. But in some cases cogging torque appears due to the spatial periodicity of the magnetic structure [5].

Cogging torque, a periodic oscillation torque, is due to energy variation within a motor as the rotor turns, even if there is no current in the windings [6,7], with the tendency of the rotor field to align with the stator poles. The combination of cogging torque and torque ripple causes unstable torque pulsation [8,9], which results in additional and undesired vibration and noise during machine operation [10]. Thus, when PMSMs are used in high-accuracy position control and/or constant speed control, such as in robots and hard disk machine drives, one must solve the cogging torque problem [11]. The precise analysis and evaluation of the cogging torque needs numerous detailed partitioned meshes when applying the finite element method (FEM) because the magnetic flux density distribution varies drastically in the air-gap of PMSM. However, this requires excessive computing time and memory size, which are unacceptable for the design and performance improvement of large machines or machines with a large number of poles and slots.

Reduction of cogging torque has been done in many ways for a long time, such as skewing rotor and/or stator slot positions, modification of slot-opening width, fractional-slot stator, notches on the stator face, uneven distribution of stator slots, changes in the ratio of stator alveolar position, the size or width of magnets, as well as changes in the magnetization direction of the magnetic pole, asymmetrical structures arrangement of rotor poles, increase in the number of slots per pole, and others [12–16]. However, as the related publications appeared in the literature are concerned, the comparisons between the aforementioned methods the studies on their effectiveness are insufficient so far.

The goal of this paper is to study the occurrence of cogging torque, and to propose a novel rapid method, the so-called half magnetic pole pair (HMPP) analysis, for forecasting and evaluating the cogging torque. In accordance with the method, first the permanent magnet of a rotor is geometrically partitioned into regions of interest for a subsequent Maxwell-2D analysis run by FEM. Calculation of the cogging torque with Matlab is then conducted. The process is executed, and total analysis time is much shorter than that of conventional techniques. Rotor skewed structures have been examined for small as well as large PMSMs to demonstrate the effectiveness of the proposed method.

The paper is organized as follows: Section 2 introduces the existence and evaluation technique of cogging torque theoretically; Section 3 presents the principle of the HMPP analysis for evaluating cogging torque, and uses a PMSM to demonstrate the method; Section 4 applies the novel HMPP method to analyze and predict the cogging torque of a multi-pole and slotted, large-capacity wind generator using the skewed technique directly to reduce the cogging torque. Finally, conclusions are presented in Section 5.

2. Derivation of Cogging Torque

Hanselman described that PMSM can be modeled by a permanent magnet and an exciting coil. The electromagnetic torque in PMSM includes cogging torque and a correction component. In a magnetic circuit composed of a permanent magnet and an exciting coil, the co-energy is shown in Equation (1), where the first to third terms correspond to the co-energies of the self-inductance, the permanent

magnet, and that due to mutual flux, respectively [8]. The electromagnetic torque T can then be derived by differentiating the magnetic field energy W or total co-energy W_c with respect to mechanical angle, as is shown in Equation (2):

$$W_c = \frac{1}{2} Li^2 + \frac{1}{2} (\mathfrak{R} + \mathfrak{R}_m) \phi_m^2 + Ni\phi_m \quad (1)$$

$$T = \left. \frac{\partial W_c}{\partial \theta} \right|_{i=\text{constant}} \quad (2)$$

where \mathfrak{R} and \mathfrak{R}_m are the reluctances seen by the magneto-motive-force source and the magnetic field, respectively; while ϕ_m is the magnetic flux of the magnet linking the exciting coil.

By substituting (1) into (2), the torque can then be calculated as:

$$T = \frac{1}{2} i^2 \frac{dL}{d\theta} - \frac{1}{2} \phi_m^2 \frac{d\mathfrak{R}}{d\theta} + Ni \frac{d\phi_m}{d\theta} \quad (3)$$

The second term in (3) is proportional to the square of the magnetic flux and is not a function of the polarity of the flux, whereas the negative sign represents that the inductance and reluctance are inversely proportional, *i.e.*, $L = N^2 / \mathfrak{R}_m$. Since the coil inductance is constant, independent of the rotating position θ , in case of lacking any exciting current, $i = 0$, only the second term will be present in (3). Thus one can evaluate the cogging torque by focusing on the magnetic interaction as well as the reluctance change between the coil and magnet, which yields:

$$T_{cog} = -\frac{1}{2} \phi_g^2 \frac{d\mathfrak{R}}{d\theta} \quad (4)$$

It is seen from (4) that the cogging torque is determined by the air-gap ϕ_g and the variation of reluctance in the magnetic circuit with the rotating displacement. That is, cogging torque appears whenever magnet flux travels through a varying reluctance.

For a geometrically symmetrical structured permanent magnet motor, cogging torque represents a periodical waveform distribution with respect to the mechanical degrees of rotation. As given in (5), the period of cogging torque in mechanical degrees is determined through dividing 360° , the overall circular mechanical degrees in space, by the least common multiple of the magnetic pole number N_p and the slot number N_s of the PMSM. Physically, cogging torque exists and causes a jogging and unsmooth motion when the shaft is rotated manually even if the PMSM has not been activated [11]. That is why the cogging torque had better be minimized during the motor design process. Equation (5) will be applied in Section 3 for determining the period of the cogging torque:

$$\theta_{cog\text{-period}} = \frac{360^\circ}{lcm(N_p, N_s)} \quad (5)$$

3. Principle of HMPP Analysis for Evaluating Cogging Torque

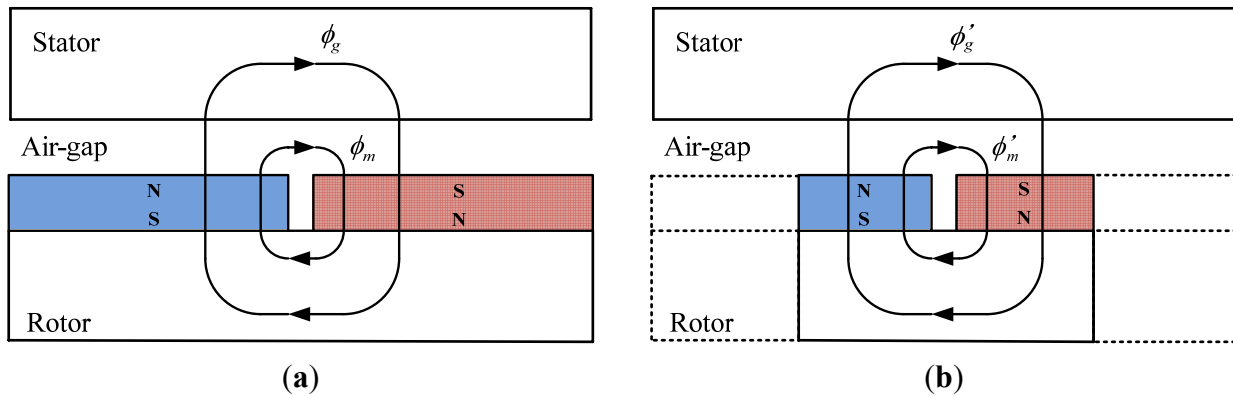
In this section, first the derivation and formulation of HMPP together with an example will be given to explain the evaluation procedure. The analytical model for cogging torque of HMPP is then

simulated and compared with conventional methods. By skewing the rotor structures, the cogging torque in machines can be reduced greatly, and thus can be implemented conveniently in manufacturing.

3.1. Definition of HMPP and Reproduction of the Cogging Torque

Analysis of the magnetic circuit requires only two adjacent half poles of the different magnetic pole faces in a rotor, because the magnetic flux travels from the rotor surface through the air-gap, the magnetic silicon steel in the stator, the air-gap, and then back to the rotor to form a complete closed-loop, as shown in Figure 1(a). Therefore, the PMSM rotor magnet under investigation, after even partitioning, could be modeled to consist of two adjacent half magnets, resulting in a half magnetic pole pair. Only half of the original volume is required for FEM, such as the region enclosed by the solid-lines, including the corresponding air-gap region of Figure 1(b).

Figure 1. Schematic diagram of PMSM: (a) magnetic flux path, (b) definition of half magnetic pole pairs.



After proper partitioning, one can use the professional software Maxwell-2D based on FEM to find the cogging torque waveform that occurs when the HMPP completes a slot pitch rotation, $360^\circ/N_s$, and to store the parameter data as tables.

The angular displacement for each HMPP is $360^\circ/N_p$ in mechanical degrees, while the mechanical angle between adjacent teeth slots is $360^\circ/N_s$. The difference between these two parameters is defined as the accumulated angle of the cogging torque, θ_δ . Thus:

$$\theta_\delta = \left| \frac{360^\circ}{N_p} - \frac{360^\circ}{N_s} \right| = 360^\circ \left| \frac{(N_s - N_p)}{N_p N_s} \right| \tag{6}$$

If N_p and N_s have the biggest common factor k , let $N_p = kX$ and $N_s = kY$, then:

$$\theta_\delta = 360^\circ \frac{k(Y - X)}{XYk^2} = 360^\circ \frac{(Y - X)}{XYk} \tag{7}$$

and the n -th accumulated angle for the HMPP is:

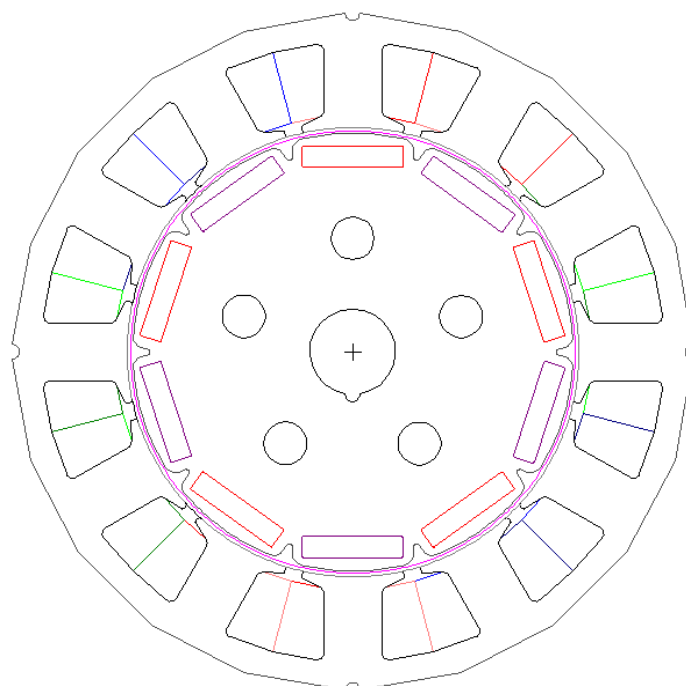
$$\theta_{\delta n} = 360^\circ \frac{(Y - X)}{XYk} (n - 1), \quad n = 1 \sim N_p \tag{8}$$

Obviously, the cogging torque will repeat periodically with $lcm(N_p, N_s)$ cycles per revolution or period in mechanical angle $\theta_{cog\text{-period}}$. The cogging torque analysis needs only to focus on the HMPP travelling in a slot pitch for every accumulated angle to simulate the magnetic interaction between each HMPP and stator teeth, that is, one just needs to calculate each corresponding accumulated angle θ_δ , of total order N_p/k over the $(N_p/k) \times \theta_\delta$ regions. The total number of accumulated calculations can be determined from slot pitch and accumulated angle, $360^\circ/N_s/\theta_\delta$. Then each accumulated angle and a typical cogging torque numerical data set for a HMPP gained earlier by Maxwell-2D software are fed into the Matlab tool software. By means of Simulink and module blocks built in Matlab, one can superimpose the corresponding cogging torque due to each accumulated angle and multiply it by k to reproduce a complete true cogging torque contributed by the permanent magnets and the teeth in the stator. Sometimes the analysis and calculation work using traditional FEM can be reduced for symmetrical structure machines, but the full model simulation is needed for asymmetrical structures. However the HMPP analysis requires only focusing on $(N_p/k) \times \theta_\delta$ regions, instead of the full motor, resulting in a noticeable reduction both in calculation work and execution time.

3.2. Finite Element Method of HMPP in Cogging Torque Analysis

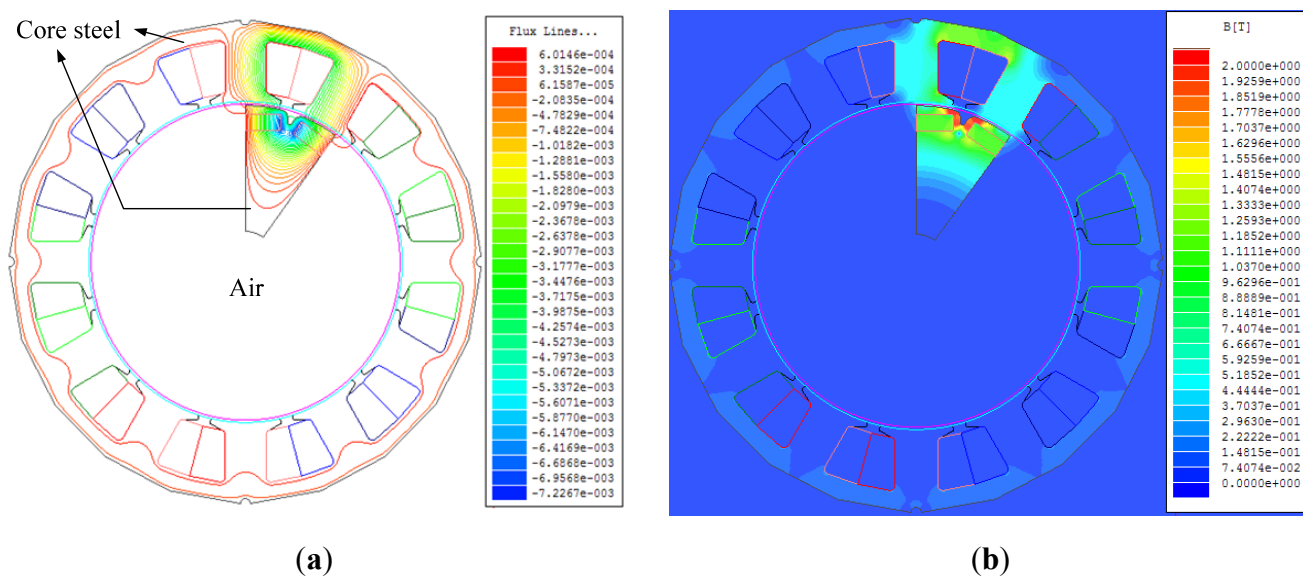
FEM is widely used in the design of electrical machines. In FEM, one can first determine the required accuracy and the corresponding number of nodes, connected lines and analysis meshes. FEM calculation is then executed for each mesh to yield performance values such as magnetic density, torque, *etc.* [17–26]. An example is shown in Figure 2. Here a 10-pole, 12-slot PMSM having 1000 mm axial length of inner rotor is set up from laminating steel sheets, and stator windings are connected for three-phase operation. First, the least common multiple, $lcm(12, 10)$, is 60 and the period of the cogging torque is 6° .

Figure 2. Structure of a 10-pole, 12-slot PMSM.



In using Maxwell-2D for the finite element analysis of the PMSM under consideration, Natural and Neumann boundaries are usually given as default boundary conditions, where Natural boundaries are assigned to the surfaces between objects, while Neumann boundaries are assigned to the outside edges of the problem region. In this example, the surfaces between core steel and air are assigned, resulting in Neumann boundaries. On the other hand, the surface between permanent magnets and core steels in the rotor are specified as the Natural boundaries. The flux plot from finite element analysis of HMPP using Maxwell-2D shown in Figure 3 verifies the aforementioned argument concerning boundary conditions.

Figure 3. Schematic diagram of magnetic field: (a) magnetic field lines; (b) flux density.



To demonstrate the approach concerning the application of HMPP to simulate the cogging torque, consider Figure 4, where three different positions of HMPP with the same mesh partition are investigated.

Figure 4. The HMPP in different mechanical angle positions and cogging torque waveforms: (a) 0 degree; (b) 72 degrees; and (c) 144 degrees.

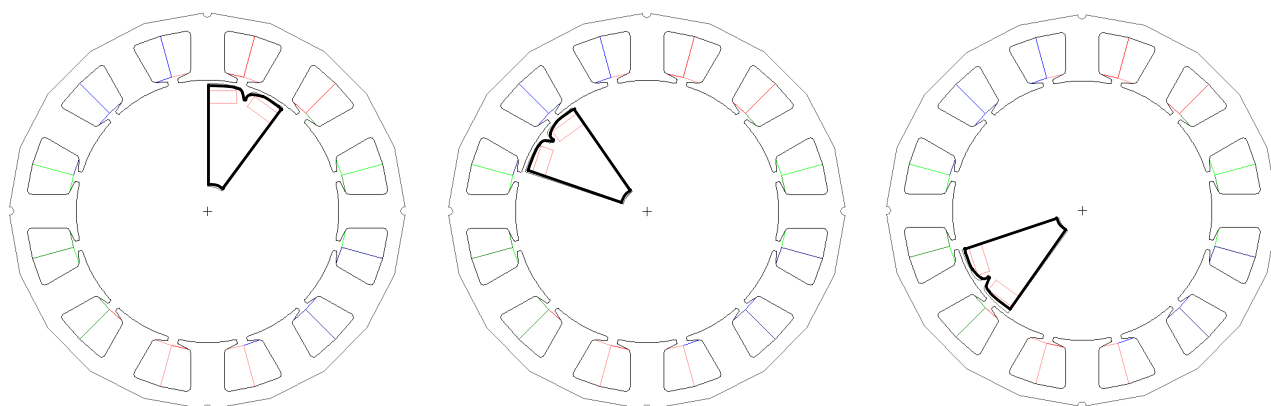
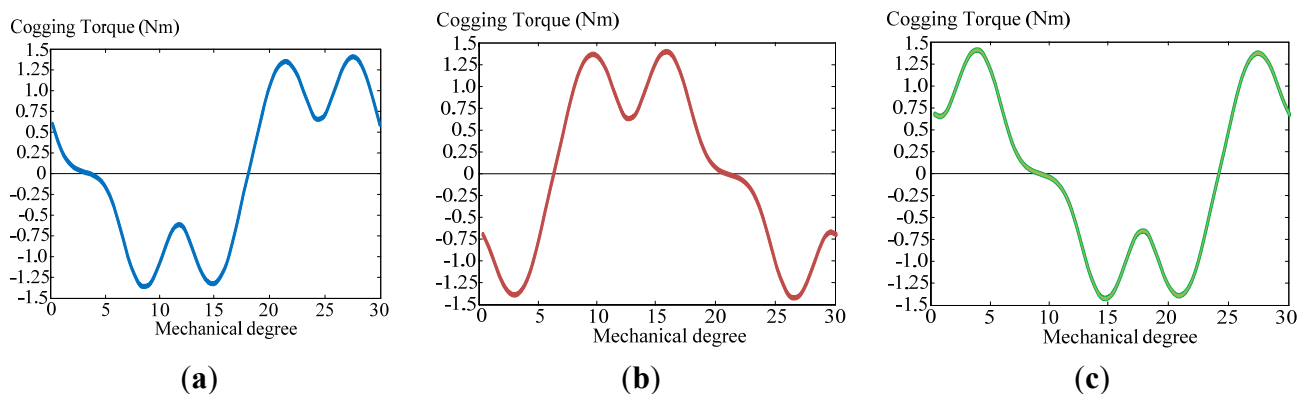


Figure 4. Cont.



The resulting cogging torque waveform distributions from Maxwell-2D differ only slightly in peak values. Thus one could pick any group of HMPP and its corresponding torque waveform in Figure 4 as the basic HMPP and torque waveform. In this paper, Figure 4(a) is chosen to proceed the following-up calculation, *i.e.*, rotate the HMPP and torque waveform obtained from 0° to 180° for every $360^\circ/N_s$, in this case 30 mechanical degrees, to get six repeated waveforms as shown in Figure 5(a). Finally, the individual cogging torque distributions are combined using Matlab to attain the complete cogging torque produced by the first HMPP. Details are given in the next paragraph.

In this example, the accumulated angle θ_δ in Equation (6) is 6° , the biggest common factor k is 2, $X = 5$, and $Y = 6$. Although there exists 10 groups of HMPP, indeed, as indicated above, the cogging torque waveform will repeat for every 30° mechanical degrees as can be seen from Figure 5(a), with the peak values of 1.4 Nm and -1.35 Nm in magnitude. Thus only five accumulated mechanical angles, *i.e.*, 0° , 6° , 12° , 18° and 24° , should be carried out using the Matlab calculation as shown in Figure 5(b) and Table 1. In addition, it is obvious from Table 1 that one only has to double the cogging torque to produce the complete cycle of the resultant cogging torque due to 10 accumulated angles. The result is given in Figure 6(a).

Figure 5. Cogging torque of HMPP for a 10-pole, 12-slot PMSM: (a) 0 degree; (b) 5 accumulated mechanical angles.

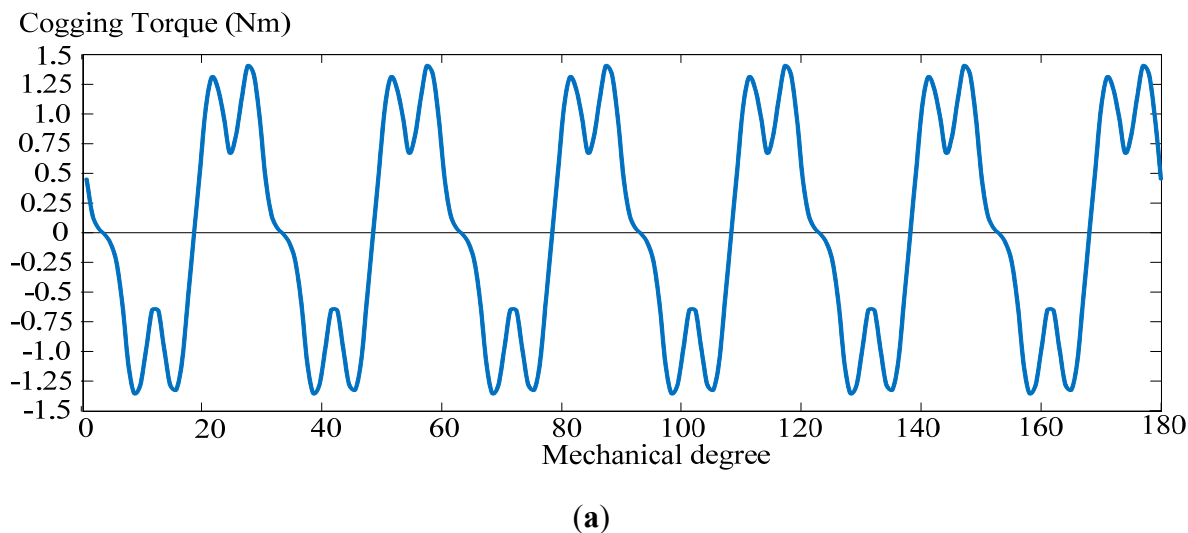
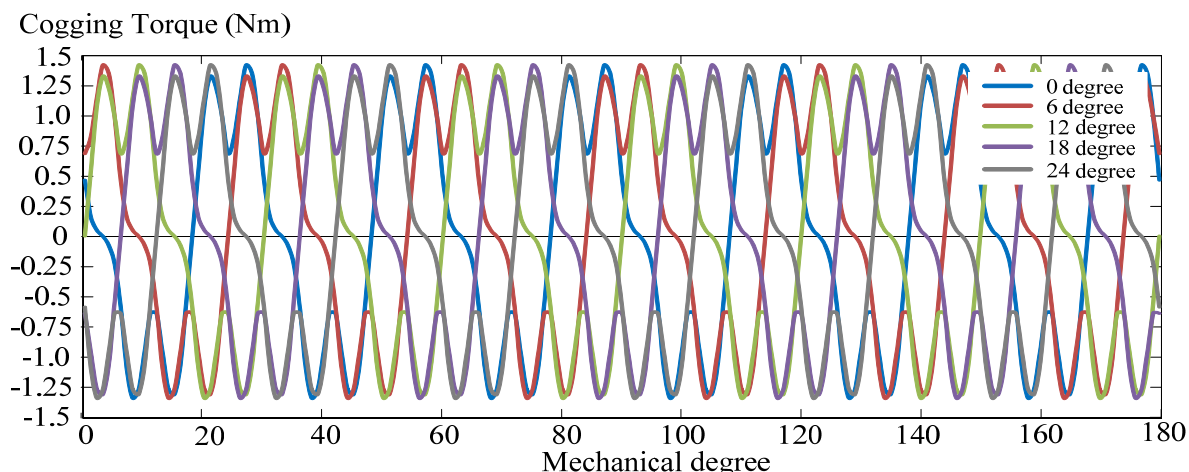


Figure 5. Cont.



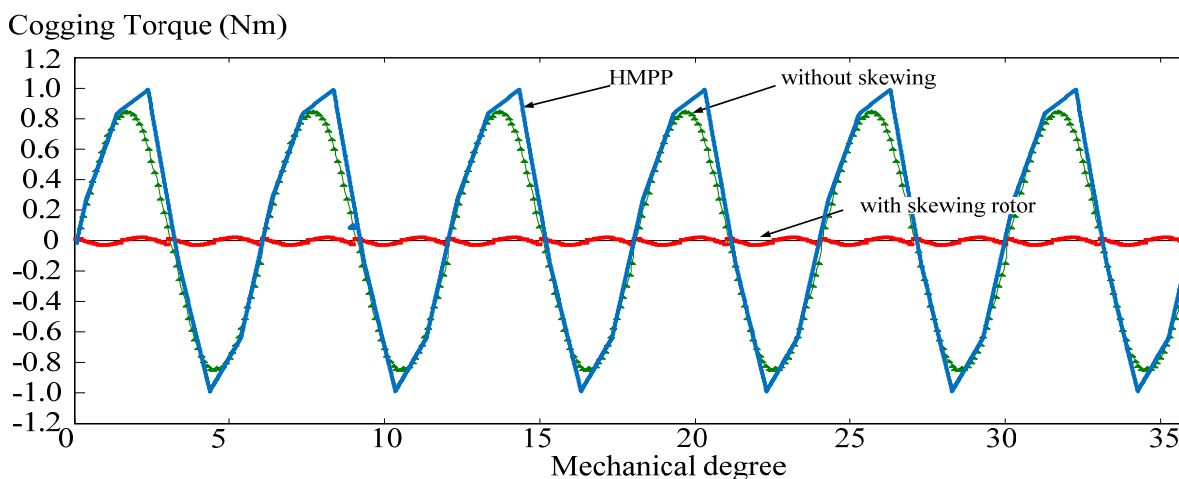
(b)

Table 1. Accumulated angle of 10-pole, 12-slot PMSM.

Poles order \ Accumulated angle	1	2	3	4	5	6	7	8	9	10
Original mechanical degree (°)	0	6	12	18	24	30	36	42	48	54
Partitioned mechanical degree (°)	0	6	12	18	24	0	6	12	18	24

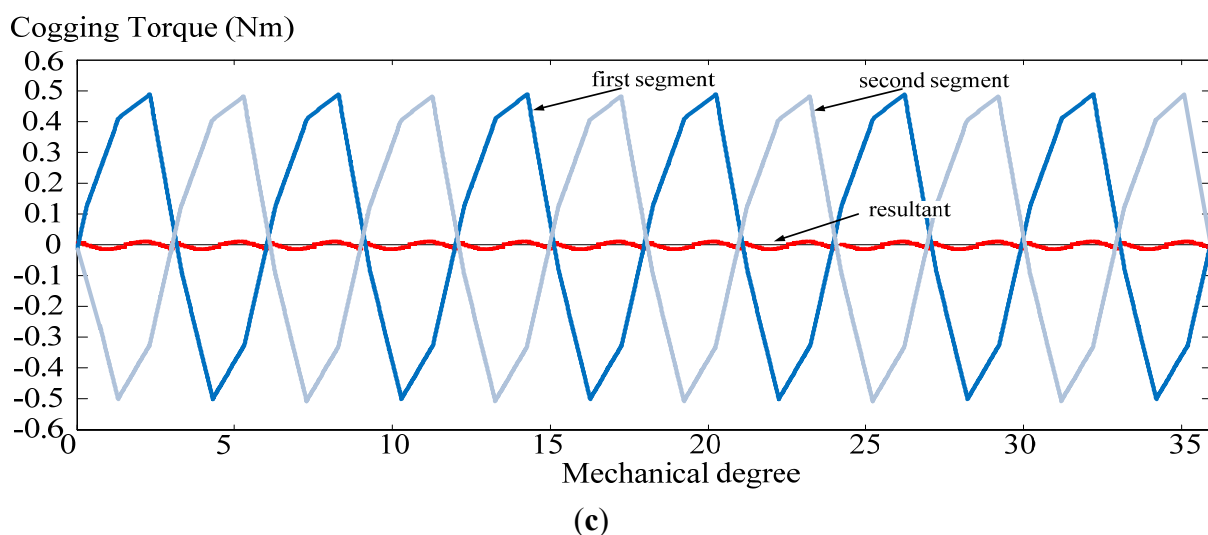
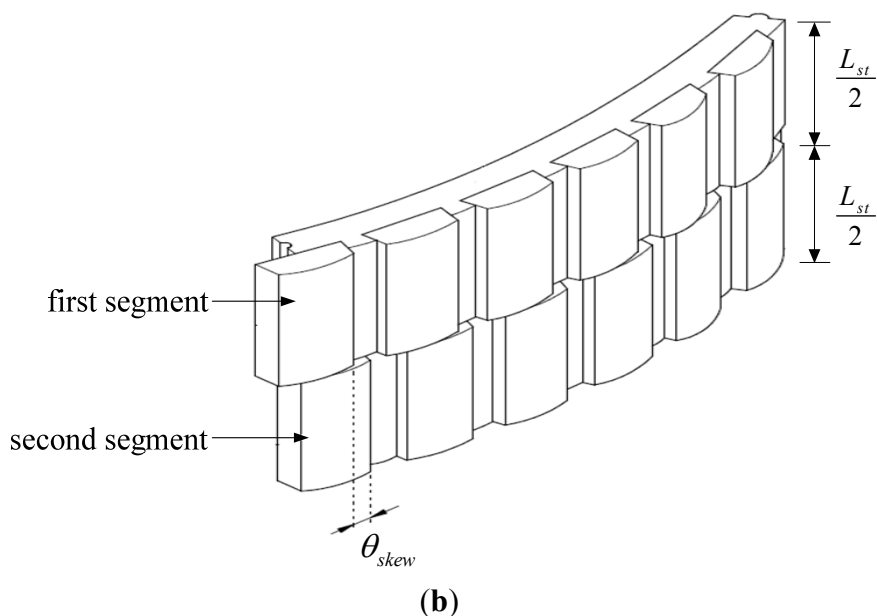
Figure 6(a) shows the cogging torque experienced when the rotor rotates through 1/10 of a complete revolution in space (60 cycles of cogging torque in 360 mechanical degrees), which covers 36° and represents six cycles. On the other hand, the originally designed rotor structure is simulated to obtain the cogging torque by directly using FEM under the full-machine model. The total execution time for the cogging torque evaluation takes 15 min to finish with the peak-to-peak value of 1.7 Nm.

Figure 6. Cogging torque experienced in 1/10 revolution: (a) comparison between full model and HMPP; (b) two-segment rotor structure; (c) component and resultant cogging torques with skewing rotor.



(a)

Figure 6. Cont.



Under all the same machine parameters, the proposed method takes only 10 min, saving a third of the above calculation time, and the peak-to-peak value is 2 Nm. It is obvious in Figure 6(a) that both waveforms represent periodical varying characteristic, with little deviation in magnitude from each other.

Skewing the rotor is one of many effective ways to reduce cogging torque. The rotor is divided into several cylindrical segments of equal length. When adjacent segments are rotated on their axis by a constant angle [3,27–29], the period of the cogging torque can be determined from Equation (5). If the machine has a two-segment rotor structure, the skew angle displacement of one-half cogging torque period is the best angle to reduce the cogging torque [28]. This will further be verified by the proposed approach to show the effectiveness of the method.

Figure 6(b) shows a two-segment rotor structure made by skewing the rotor with a one-half cogging torque period given by Equation (5), in this example, three mechanical degrees. The corresponding two cogging torques with a counter-acting effect are given in Figure 6(c), resulting in a very small overall cogging torque with the peak-to-peak value of 0.05 Nm. There is a noticeable reduction of 97.5% with

respect to the 2 Nm value obtained from the proposed HMPP analysis. A significant improvement benefit using skewing rotor has been proved quantitatively. It thus is an effective way to minimize the undesirable cogging torque.

Therefore, the novel method proposed is favorable for evaluating the existence and influence of cogging torque, especially for large-scale rotating machines or wind turbine generators, which are usually designed with a large number of poles and slots. The evaluating process is very fast and the total operation time to analyze can be lessened, taking only 2/3 as much time as full model calculation in traditional FEM analysis as mentioned above. This is a very useful and timesaving calculation method.

4. Application of the Novel HMPP Method to Analysis of Wind Generator

Most software available today was developed based on medium and/or small-capacity machines, and cannot simulate corresponding performances of large-capacity wind generators with many poles and slots. The undesired phenomena, including cogging torque, should be analyzed and evaluated quantitatively in order to pursue effective techniques to minimize any disadvantageous problems. As an example, a wind generator with 100-pole, 96-slot, 60 mm stacked length, and the relevant specifications of the generator listed in Table 2, cannot be simulated with commercial software to get its operational performance.

Table 2. Dimensions of initially designed wind generator.

Number of phase	3
Number of slots	96
Number of poles	100
Rated speed (rpm)	90
Rated output power (W)	3000
Rated torque (Nm)	318.17
Back-emf (V)	215.4
Winding turns per slot (turns)	18
Winding conductor diameter (mm)	1.0
Stator diameter inner/outer (mm)	720/800
Rotor diameter inner/outer (mm)	670/716
Air-gap length (mm)	2
Stack length (mm)	60
Core material/Permanent magnet	50CS400/NdFeB35

Figure 7 shows the stator and rotor structure after partitioning the geometric structure into HMPP for the novel (Maxwell-2D+Matlab) analysis. The meshes partitioned based on the FEM technique have been given serious and detailed consideration to yield precise analysis of the stator and rotor, resulting in data every 0.005° on average for one iterative calculation. The pole pitch of every HMPP is 3.6° , while the teeth slot pitch is 3.75° . That is, the second group of HMPP is positioned 3.6° away from the first group of HMPP, and the second group of HMPP is leading the corresponding second group of stator teeth by an accumulated angle of 0.15° . Thus, the analysis is focused on every 3.75 mechanical degrees ($0.15 \times 100/4$) so that only 25 calculations are needed as shown in Table 3.

Figure 7. A group of HMPP geometry of the 100-pole, 96-slot machine.

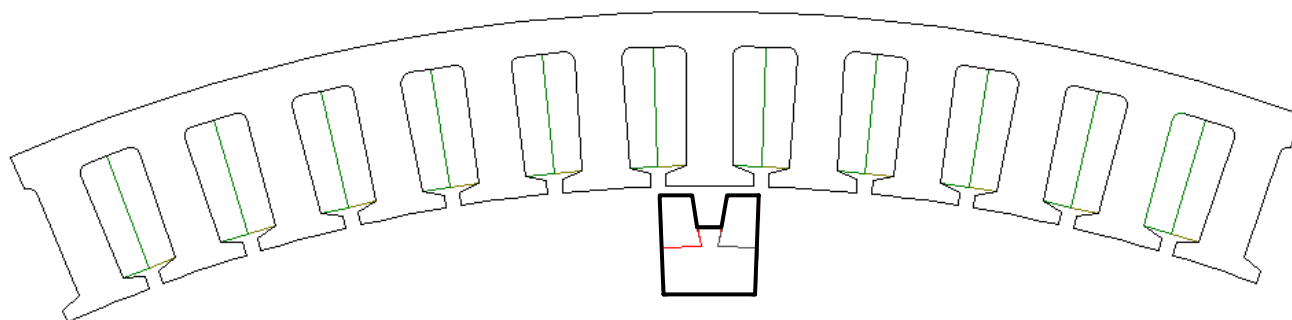


Figure 8 shows that the basic cogging torque chosen from a HMPP group rotating through 15° and analyzed by Maxwell-2D has a peak-to-peak value of 4.8 Nm. Now let the typical cogging torque be a basis, shift the basis according to the accumulated angles θ_0 given in Table 3, and then superimpose with the data Matlab manipulation. The resultant waveform is given in Figure 9, which shows the true complete cogging torque waveform of the wind generator with a peak-to-peak value of 0.054 Nm.

Figure 8. Typical cogging torque of HMPP of 100-pole, 96-slot machine.

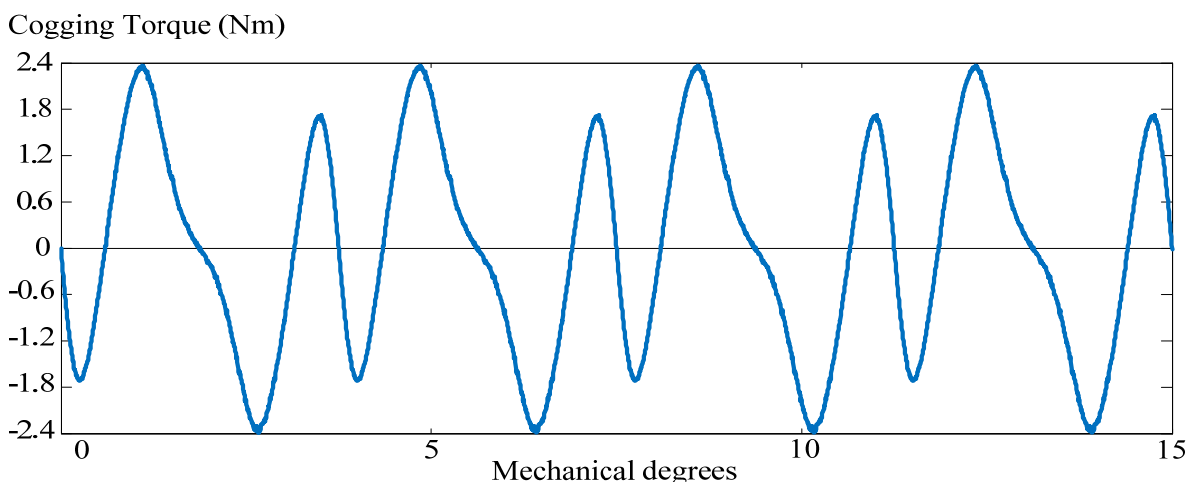


Figure 9. Complete cogging torque of 100-pole, 96-slot machine manipulated by Matlab.

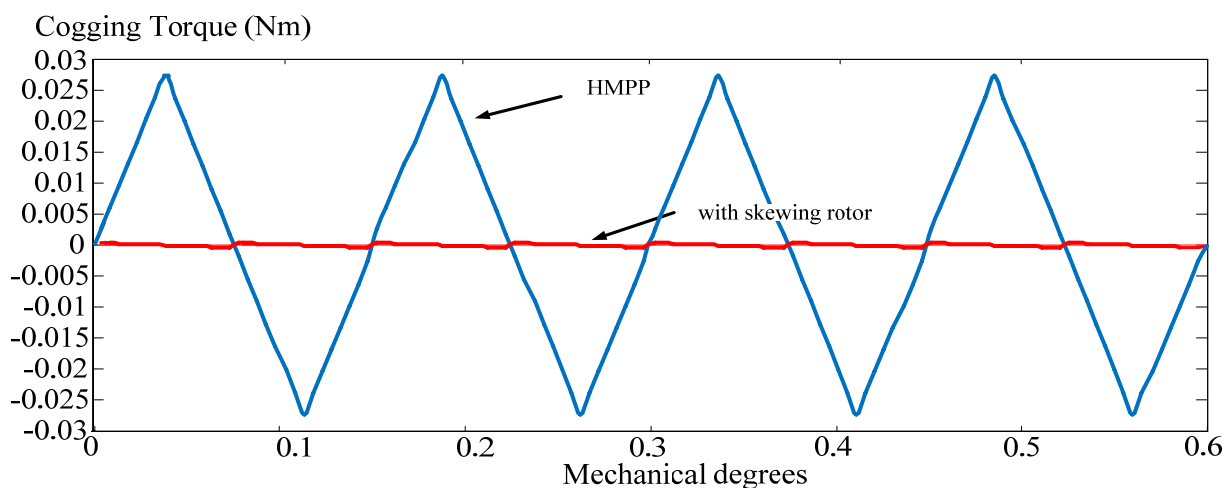


Table 3. Mechanical degrees of 100-pole and 96-slot.

Poles order	1	2	3	4	5	6	7	8	9	10	11	12
Accumulated angle												
Mechanical degrees (°)	0	0.15	0.3	0.45	0.6	0.75	0.9	1.05	1.2	1.35	1.5	1.65
Poles order	13	14	15	16	17	18	19	20	21	22	23	24
Accumulated angle												
Mechanical degrees (°)	1.8	1.95	2.1	2.25	2.4	2.55	2.7	2.85	3	3.15	3.3	3.45
Poles order	25...											
Accumulated angle												
Mechanical degrees (°)	3.6	3.75→0, 3.9→0.15, 4.05→0.3, 4.2→0.45... ..and so on.										

The total time used for the computer analysis is 60 min. After skewing the rotor with a one-half cogging torque period given by Equation (5), the peak-to-peak value of the cogging torque is 0.0007 Nm and a 98.7% reduction in cogging torque is obtained; thereby an effective mean for minimizing cogging torque can be evaluated and verified.

Table 4 lists the analysis results using the novel HMPP method proposed in this paper. The traditional FEM analysis cannot be executed due to the limited meshes used by the Maxwell-2D software, although many more meshes with a very expensive and supercomputer could be used. Thus, conventionally there is no way to foresee or evaluate the magnitude of cogging torque and its impact on large-capacity machines.

Table 4. Cogging torque obtained from the proposed HMPP method of the 100-pole, 96-slot wind generator.

	HMPP
Cogging torque analysis	0.054 Nm _(pp)
Total process time	60 min.
Cogging torque with skewing rotor	0.0007 Nm _(pp)
Cogging torque reduction	98.7%

The novel HMPP method proposed in this paper takes less than 60 min with pronounced improvement prediction of the cogging torque. In addition, one can find and verify the effectiveness for every possible means to improve the operational characteristics, which were not executable before.

5. Conclusions

In this paper, a novel and fast HMPP design evaluation technique has been proposed. The method is set up by combining FEM and Matlab software, and it provides a rapid evaluation tool for analyzing the cogging torque quantitatively. The results are reasonable and acceptable, both in execution time and accuracy. By using the HMPP method, designers can anticipate the distribution of cogging torque and verify the effectiveness of possible techniques for reducing cogging torque, which was impossible before, especially for the analysis of large machines or machines with a large number of poles and slots. Examples of skew rotors are examined in this paper to justify the feasibility of the proposed method for calculating and reducing cogging torque.

References

1. Kang, G.H.; Son, Y.D.; Kim, G.T.; Hur, J. A novel cogging torque reduction method for interior-type permanent-magnet motor. *IEEE Trans. Ind. Appl.* **2009**, *45*, 161–167.
2. Güemes, J.A.; Iraolagoitia, A.M.; del Hoyo, J.I.; Fernández, P. Torque analysis in permanent-magnet synchronous motors: A comparative study. *IEEE Trans. Energy Convers.* **2011**, *26*, 55–63.
3. Islam, R.; Husain, I.; Fardoun, A.; McLaughlin, K. Permanent-magnet synchronous motor magnet designs with skewing for torque ripple and cogging torque reduction. *IEEE Trans. Ind. Appl.* **2009**, *45*, 152–160.
4. EL-Refaie, A.M. Fractional-slot concentrated-windings synchronous permanent magnet machines: Opportunities and challenges. *IEEE Trans. Ind. Electron.* **2010**, *57*, 107–121.
5. Popescu, M.; Cistelecan, M.V.; Melcescu, L.; Covrig, M. Low Speed Directly Driven Permanent Magnet Synchronous Generators for Wind Energy Applications. In *Proceedings of the International Conference on Clean Electrical Power*, Capril, Italy, 21–23 May 2007; pp. 784–788.
6. Wang, Y.; Jin, M.J.; Fei, W.Z.; Shen, J.X. Cogging torque reduction in permanent magnet flux-switching machines by rotor teeth axial pairing. *IET Electric Power Appl.* **2010**, *4*, 500–506.
7. Wang, D.; Wang, X.; Qiao, D.; Pei, Y.; Jung, S.-Y. Reducing cogging torque in surface-mounted permanent-magnet motors by nonuniformly distributed teeth method. *IEEE Trans. Magn.* **2011**, *47*, 2231–2239.
8. Hanselman, D. *Brushless Permanent Magnet Motor Design*; Magna Physics Pub: Orono, ME, USA, 2003.
9. Islam, M.S.; Islam, R.; Sebastian, T. Experimental verification of design techniques of permanent-magnet synchronous motors for low-torque-ripple applications. *IEEE Trans. Ind. Appl.* **2011**, *47*, 88–95.
10. Ho, S.L.; Chen, N.; Fu, W.N. An optimal design method for the minimization of cogging torques of a permanent magnet motor using FEM and genetic algorithm. *IEEE Trans. Appl. Supercond.* **2010**, *20*, 861–864.
11. Hendershot, J.R.; Miller, T.J.E. *Design of Brushless Permanent Magnet Motors*; Oxford University Press: New York, NY, USA, 1994.
12. Bianchi, N.; Bolognani, S. Design techniques for reducing the cogging torque in surface-mounted PM motors. *IEEE Trans. Ind. Appl.* **2002**, *38*, 1259–1265.
13. Dai, M.; Keyhani, A.; Sebastian, T. Torque ripple analysis of a PM brushless DC motor using finite element method. *IEEE Trans. Energy Convers.* **2004**, *19*, 40–45.
14. Zhu, Z.Q.; Howe, D. Influence of design parameters on cogging torque in permanent magnet machines. *IEEE Trans. Energy Convers.* **2000**, *15*, 407–412.
15. Sooriyakumar, G.; Perryman, R.; Dodds, S.J. Cogging Analysis for Fractional Slot/Pole Permanent Magnet Synchronous Motors. In *Proceedings of the 42nd International Universities Power Engineering Conference*, Brighton, UK, 4–6 September 2007; pp. 188–191.
16. Wang, D.; Wang, X.; Yang, Y.; Zhang, R. Optimization of magnetic pole shifting to reduce cogging torque in solid-rotor permanent-magnet synchronous motors. *IEEE Trans. Magn.* **2010**, *46*, 1228–1234.

17. Ohnishi, T.; Takahashi, N. Optimal design of efficient IPM motor using finite element method. *IEEE Trans. Magn.* **2000**, *36*, 3537–3539.
18. Pern, J.-F.; Yeh, S.-N. Calculating the current distribution in power transformer windings using finite element analysis with circuit constraints. *IEE Proc. Sci. Meas. Technol.* **1995**, *142*, 231–236.
19. Chen, C.-Y.; Yeh, S.-N. An improved finite element method for electromagnetic field analysis. *J. Chin. Instit. Electr. Eng.* **1996**, *3*, 245–251.
20. Chen, C.-Y.; Yeh, S.-N. An improved finite element method for induction motor analysis. *J. Chin. Inst. Electr. Eng.* **1996**, *3*, 27–36.
21. Lefèvre, Y.; Fontchastagner, J.; Messine, F. Building a CAD system for educational purpose based only on a mesh tool and a finite elements solver. *IEEE Trans. Magn.* **2006**, *42*, 1483–1486.
22. Kim, K.-C.; Lee, J.; Kim, H.-J.; Koo, D.-H. Multiobjective optimal design for interior permanent magnet synchronous motor. *IEEE Trans. Magn.* **2009**, *45*, 1780–1783.
23. Andriollo, M.; de Bortoli, M.; Martinelli, G.; Morini, A.; Tortella, A. Design improvement of a single-phase brushless permanent magnet motor for small fan appliances. *IEEE Trans. Ind. Electron.* **2010**, *57*, 88–95.
24. Van der Giet, M.; Lange, E.; Corrêa, D.A.P.; Chabu, I.E.; Nabeta, S.I.; Hameyer, K. Acoustic simulation of a special switched reluctance drive by means of field–circuit coupling and multiphysics simulation. *IEEE Trans. Ind. Electron.* **2010**, *57*, 2946–2953.
25. Cho, H.-W.; Ko, K.-J.; Choi, J.-Y.; Shin, H.-J.; Jang, S.-M. Rotor natural frequency in high-speed permanent-magnet synchronous motor for turbo-compressor application. *IEEE Trans. Magn.* **2011**, *47*, 4258–4261.
26. Li, G.J.; Ojeda, J.; Hoang, E.; Gabsi, M. Thermal-electromagnetic analysis of a fault-tolerant dual-star flux-switching permanent magnet motor for critical applications. *IET Electric Power Appl.* **2011**, *5*, 503–513.
27. Borghi, C.A.; Casadei, D.; Cristofolini, A.; Fabbri, M.; Serra, G. Minimizing torque ripple in permanent magnet synchronous motors with polymer-bonded magnets. *IEEE Trans. Magn.* **2002**, *38*, 1371–1377.
28. Chen, H.-S.; Dorrell, D.G.; Tsai, M.-C. Design and operation of interior permanent-magnet motors with two axial segments and high rotor saliency. *IEEE Trans. Magn.* **2010**, *46*, 3664–3675.
29. Jiabin, W.; Yabin, P. Research of Six-Pole Permanent Magnet Submersible Motor Design. In *Proceedings of the 6th International Forum on Strategic Technology*, Harbin, China, 22–24 August 2011; pp. 545–548.